Soft Matter

Accepted Manuscript

ROYAL SOCIETY OF CHEMISTRY

www.rsc.org/softmatter

ARTICLE TYPE www. rsc.org/xxxxxx | XXXXXXXX

Motility versus fluctuations in mixtures of self-motile and passive agents

Denis F. Hinz,[a] Alexander Panchenko,[b] Tae-Yeon Kim,[c] and Eliot Fried[d‡]

Received Xth XXXXXXXXXX 20XX, Accepted Xth XXXXXXXXX 20XX
First published on the web Xth XXXXXXXXXX 200X
DOI: 10.1039/b000000x

Many biological systems consist of self-motile and passive agents both of which contribute to overall functionality. However, little is known about the properties of such mixtures. Here we formulate a model for mixtures of self-motile and passive agents and show that the model gives rise to three different dynamical phases: a disordered mesoturbulent phase, a polar flocking phase, and a vortical phase characterized by large-scale counterrotating vortices. We use numerical simulations to construct a phase diagram and compare the statistical properties of the different phases with observed features of self-motile bacterial suspensions. Our findings afford specific insights regarding the interaction of microorganisms and passive particles and provide novel strategic guidance for efficient technological realizations of artificial active matter.

1 Introduction

Individual agents capable of directed movement are usually referred to as active, self-propelled, or self-motile. This capacity leads to remarkable features of bacterial suspensions, *in-vitro* networks of protein filaments, and the cytoskeletons of living cells. Likewise, macroscopic active systems, such as animal colonies exhibit swarming, herding, and flocking behaviors that appear to share phenomenological similarities with their microscopic counterparts. Such phenomena include polar ordering, large-scale correlated motion, and intriguing rheological properties.[1] However, biological systems often consist of multiple species which differ in their motilities and other attributes. For example, the emergence of different phenotypes in microbial biofilms generates heterogeneous populations of bacteria.[2–6] In biological systems such as biofilms individual organisms die, malfunction, or lose their flagella, thereby becoming partially or completely immotile.

To elucidate the interactions between active agents and passive objects and make use of interaction phenomena for specific applications, several model systems have been studied. For example, baths of swimming bacteria,[7–11] algae,[12] and artificial self-propelled rods were found to promote an overall increase in the diffusion of suspended passive tracer particles,[11] except for very low concentrations of bacteria, where experiments and simulations suggest a decrease in diffusivity.[13] In addition, it was discovered that bacteria baths can mediate effective short range depletion-like attractions between passive suspended colloids.[14] While simulations of self-motile and passive rod-shaped agents suggest spontaneous segregation,[15] simulations of mixtures of self-propelled and passive hard spheres point at the possibility of promoting the crystallization of hard-sphere glasses through activity.[16] Recently, bacteria have been used to drive the accumulation of colloids in microstructures that are patterned with asymmetric energy barriers.[17,18] Further, simulations and experiments show that bacteria can be used to collectively move larger objects such as asymmetric micro shuttles[19] and microscopic gears and ratchets.[20,21] Similarly, surface-attached monolayers of bacteria swarms can drive microstructures[22–24] and bacteria-attached micro-beads.[25,26] Conversely, the displacement and release of small cargos of the approximately same size as the individual cargo-carrying organisms has been realized using bacteria[27] as well as algae cells.[28]

In view of these examples, insights regarding the salient biological and mechanical interactions are of great relevance to understanding biological systems and might enable progress in potential technological applications including, in particular, the design of artificial active matter systems. For example, techniques of synthetic biology and systems biology have made it possible to *fabricate* bacterial strains with

† Electronic Supplementary Information (ESI) available: The supporting movie anim_Pe_0p1_actFract_0p1.mp4 corresponds to the snapshot of the mesoturbulent phase shown in Fig. 1 (a); The supporting movie anim_Pe_1p1_actFract_0p5.mp4 corresponds to the snapshot of the flocking phase shown in Fig. 1 (b); The supporting movie anim_Pe_1p1_actFract_0p1.mp4 corresponds to the snapshot of the vortical phase shown in Fig. 1 (c). See DOI: 10.1039/b000000x/

[a] *Kamstrup A/S, Industrivej 28, Stilling, 8660 Skanderborg, Denmark.*
[b] *Department of Mathematics, Washington State University, Pullman, WA, 99164, USA.*
[c] *Civil Infrastructure and Environmental Engineering, Khalifa University of Science, Technology and Research, Abu Dhabi, 127788, UAE.*
[d] *Mathematical Soft Matter Unit, Okinawa Institute of Science and Technology, Okinawa, Japan 904-0495.*
‡ Corresponding author: Fax: +81-(0)98-966-1062; Tel: +81-(0)98-966-1381; E-mail: eliot.fried@oist.jp

Table 1 Summary of interaction forces between agents

Interaction type	Interaction force $\mathbf{f}^{ij}$	
passive ↔ passive	$\mathbf{f}^{ij}_{\mathrm{pp}} = \begin{cases} \mathbf{f}^{ij}_{\mathrm{C}} + \mathbf{f}^{ij}_{\mathrm{D}} + \mathbf{f}^{ij}_{\mathrm{R}}, & r < r_c \\ \mathbf{0}, & \text{otherwise} \end{cases}$	
active ↔ passive active ↔ active	$\mathbf{f}^{ij}_{\mathrm{ap}} = \mathbf{f}^{ij}_{\mathrm{aa}} = \begin{cases} \mathbf{f}^{ij}_{\mathrm{C}} + \mathbf{f}^{ij}_{\mathrm{D}}, & r < r_c \\ \mathbf{0}, & \text{otherwise} \end{cases}$	

engineered gene-regulation circuits that produce predefined spatial and temporal patterns.[29–34] Similarly, artificial self-motile agents can be realized through catalytically driven Janus particles,[35–39] light-activated particles,[40,41] polymer-based nanomotors,[42–44] and robotic swarms.[45–47] From a technological perspective, it is of key importance to know whether it is possible to use a small number of these potentially difficult to manufacture agents to drive other passive agents and thereby generate desirable flow patterns. Having an understanding of how many active agents are required for such a principle seems particularly crucial, as does knowing how such a principle might be realized most efficiently.

2 Model

Since most self-motile systems of biological type involve organisms with complex molecular structures, the simulation of such systems on a molecular level including all biophysical and biochemical details is inhibitively expensive, even with access to large supercomputers. In the present article we thus focus on a minimal mesoscopic (coarse-grained) description to study the salient features of generic mixtures of mesoscopic active and passive agents without accounting for details on the level of individual atoms or details of the previously discussed specific examples. Our objective therefore lies in understanding the criteria for which different dynamical phases may be observed in dense mixtures of self-motile and passive spherical soft-core agents. The motion of an agent i with constant mass m^i in a system of N agents is governed by Newton's equations for a mixture of active and passive agents

$$\left.\begin{aligned} &\dot{\mathbf{x}}^i = \mathbf{v}^i, \\ &m^i\dot{\mathbf{v}}^i = \begin{cases} \sum\limits_{j\in I_p} \mathbf{f}^{ij}_{\mathrm{pp}} + \sum\limits_{j\in I_a} \mathbf{f}^{ij}_{\mathrm{pa}}, & \text{for } i \in I_p, \\ \sum\limits_{j\in I_p} \mathbf{f}^{ij}_{\mathrm{pa}} + \sum\limits_{j\in I_a} \mathbf{f}^{ij}_{\mathrm{aa}} + \mathbf{f}^{i}_{\mathrm{F}}, & \text{for } i \in I_a, \end{cases} \end{aligned}\right\} \quad (1)$$

where I_a is the index set of active agents, I_p is the index set of passive agents, $\mathbf{f}^{ij}_{\mathrm{pp}}$ is the interaction force between passive agents, $\mathbf{f}^{ij}_{\mathrm{ap}}$ is the interaction force between active and passive agents, $\mathbf{f}^{ij}_{\mathrm{aa}}$ is the interaction force between active agents, and $\mathbf{f}^{i}_{\mathrm{F}}$ is the external force exerted on active agent i. For $\mathbf{f}^{ij}_{\mathrm{pp}}$, $\mathbf{f}^{ij}_{\mathrm{ap}}$, and $\mathbf{f}^{ij}_{\mathrm{aa}}$ the short-range interaction forces of dissipative particle dynamics (DPD) are used, with $\mathbf{f}^{ij}_{\mathrm{C}}$ the purely conservative force, $\mathbf{f}^{ij}_{\mathrm{D}}$ the purely dissipative force, and $\mathbf{f}^{ij}_{\mathrm{R}}$ the purely random force. The interaction forces corresponding to the three different interaction types passive↔passive, passive↔active, and active↔active are summarized in Table 1 with $r = |\mathbf{r}^i - \mathbf{r}^j|$ the distance between agents i and j, and with r_c the cutoff radius of the interaction forces. To model the features of a binary mixture, we apply $\mathbf{f}^{i}_{\mathrm{F}}$ only on the fraction ϕ of active agents and the random contribution of the DPD interactions $\mathbf{f}^{ij}_{\mathrm{R}}$ only between pairs of the fraction

$$\phi_p = 1 - \phi \quad (2)$$

of passive agents, as summarized in Table 1. This choice represents a suitable model for a binary mixture where the random interactions of the passive agents compete with the self-propulsion force $\mathbf{f}^{i}_{\mathrm{F}}$ of the active agents. Actual physical systems are most likely not strictly binary, since sufficiently small active agents might be subject to random interactions as well or, conversely, since sufficiently large passive agents might not be subject to random interactions. However, this depends on many parameters, including the characteristic linear dimensions, the characteristic shapes, and the characteristic masses of active and passive agents. Here, we restrict ourselves to a simple binary model system suitable to study the competition between the two different mechanisms — self-propulsion and random interactions. One conceivable physical realization of this model system corresponds to the limiting case where the passive agents are much smaller than the active agents, which is realized in experiments involving bacterial baths and smaller tracer particles discussed in the introduction.

The DPD interaction forces are taken to be of the form[48]

$$\left.\begin{aligned} \mathbf{f}^{ij}_{\mathrm{C}} &= A w(r)\hat{\mathbf{e}}^{ij}, \\ \mathbf{f}^{ij}_{\mathrm{D}} &= -\gamma w^2(r)[(\mathbf{v}^i - \mathbf{v}^j)\cdot\hat{\mathbf{e}}^{ij}]\hat{\mathbf{e}}^{ij}, \\ \mathbf{f}^{ij}_{\mathrm{R}} &= \sqrt{2\gamma k_B T} w(r)\theta^{ij}(\Delta t)^{-1/2}\hat{\mathbf{e}}^{ij}, \end{aligned}\right\} \quad (3)$$

where $w(r) = 1 - r/r_c$ is the weighting function, $\hat{\mathbf{e}}^{ij} = (\mathbf{r}^i - \mathbf{r}^j)/r$ is the unit vector directed from agent i to agent j, θ^{ij} is a random number, $A > 0$ is the conservative force parameter, and $\gamma > 0$ is the pairwise friction parameter. In $(3)_3$, k_BT, with k_B Boltzmann's constant and T the absolute temperature, provides a reference energy scale and Δt is the simulation timestep. Together with the pairwise friction parameter γ, k_BT characterizes the magnitude of the pairwise random forces accounting for fluctuations. Apart from standard DPD forces, we incorporate self-propulsion through a flocking term

$$\mathbf{f}^{i}_{\mathrm{F}} = (\alpha - \beta|\mathbf{v}^i|^2)\mathbf{v}^i, \quad (4)$$

with $\alpha \geq 0$ the constant self-propulsion force parameter and $\beta \geq 0$ the constant Rayleigh friction parameter.[49–54]

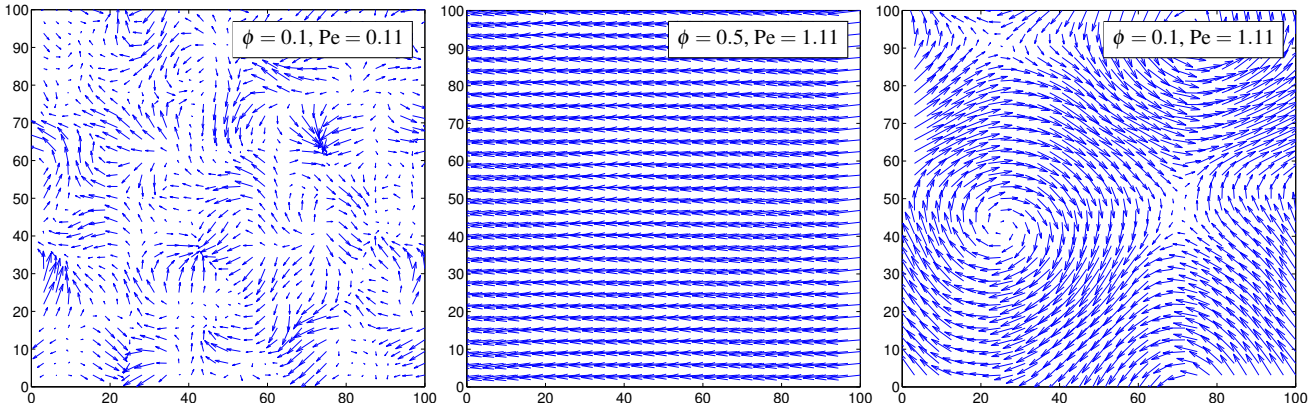

(a) Mesoturbulent **(b)** Polar flock **(c)** Vortical

Fig. 1 Coarse-grained velocity field $\mathbf{u}_M$ for $\beta = 2.25$ and representative choices of ϕ and Pe. (a) arises for small ϕ in combination with small Pe; (b) arises for intermediate and large ϕ in combination with large Pe; (c) arises for small ϕ and Pe > 1.

If all agents are passive, the motion is governed entirely by random interactions due to the equilibrium energy of the standard DPD thermostat and the energy per unit mass of the system is

$$E_R = k_B T. \tag{5}$$

Conversely, in the limit of vanishing random interactions, the flocking term (4) yields an unidirectional perfect flock in which all agents move in the same direction with the flocking velocity magnitude $v_F = \sqrt{\alpha/\beta}$ and the associated energy per unit mass of the unidirectional flocking motion is given by

$$E_F = \frac{\alpha}{2\beta}. \tag{6}$$

The limiting behavior (6) can be obtained from a modified coarse-grained Langevin equation for active agents in an effective "thermal bath" of passive agents considering the dilute limit.

Hereafter, most quantities are dimensionless and we note when a quantity carries dimensions. Working with reduced units and using the standard parameter values for a passive DPD fluid,[48] we set $m^i = 1.0$, $k_B T = 1.0$, $r_c = 1.0$, $A = 25.0$, $\gamma = 4.5$, and $\rho_{2D} = \frac{N}{L^2} = 2.5$ (two-dimensional (2D) analog of $\rho_{3D} = 4.0$), where L is the dimensionless edge length of the square computational domain. We perform simulations with LAMMPS[55,56] using periodic boundary conditions and the standard velocity-Verlet[57] time integration scheme with a dimenesionless integration timestep of $\Delta t = 3.0 \times 10^{-3}$. We run all simulations for 2.0×10^6 timesteps to ensure that the total kinetic energy of the system has stabilized near a constant value, as verified by monitoring the total energy of the system. Initially, we take all agents to be randomly distributed with zero initial velocities. Having chosen values for all previously discussed parameters, the remaining free parameters are ϕ, α, and β.

3 Phase diagram

A Péclet number that characterizes the ratio of the self-propulsion energy to the energy of random fluctuations can be defined by

$$\mathrm{Pe} = \frac{\alpha}{2\beta k_B T}. \tag{7}$$

Depending on the values of Pe and ϕ, the system develops three different dynamical phases: a disordered mesoturbulent phase, a polar flocking phase, and a vortical phase characterized by large-scale counterrotating vortices (Fig. 1). Importantly, no segregation is observed (Fig. 2 (c)–(f)). We use order parameters based on the agent velocities $\mathbf{v}^i$ and the coarse-grained vorticity $\omega = \mathrm{curl}\,\mathbf{u}_M$ to quantify the influence of ϕ and Pe on phase emergence. Given a sufficiently rapidly decaying filtering kernel, we compute the coarse-grained velocity

$$\mathbf{u}_M(\mathbf{x}_M) = \frac{1}{n}\sum_{i=1}^{N} \mathbf{v}^i \psi(\mathbf{x}_M - \mathbf{x}^i) \tag{8}$$

on a uniform grid with equidistant spacing in both coordinate directions, where n is the number of agents for which $\psi \neq 0$.

Table 2 Summary of criteria used to identify different phases

Phase	P_v	P_ω	snapshot
Mesoturbulent (T)	$P_v \to 1$	$P_\omega \to 0$	Figure 1 (a)
Polar flock (F)	$P_v \to 0$	$P_\omega \to 0$	Figure 1 (b)
Vortical (V)	$P_v \to 1$	$P_\omega > 0$	Figure 1 (c)

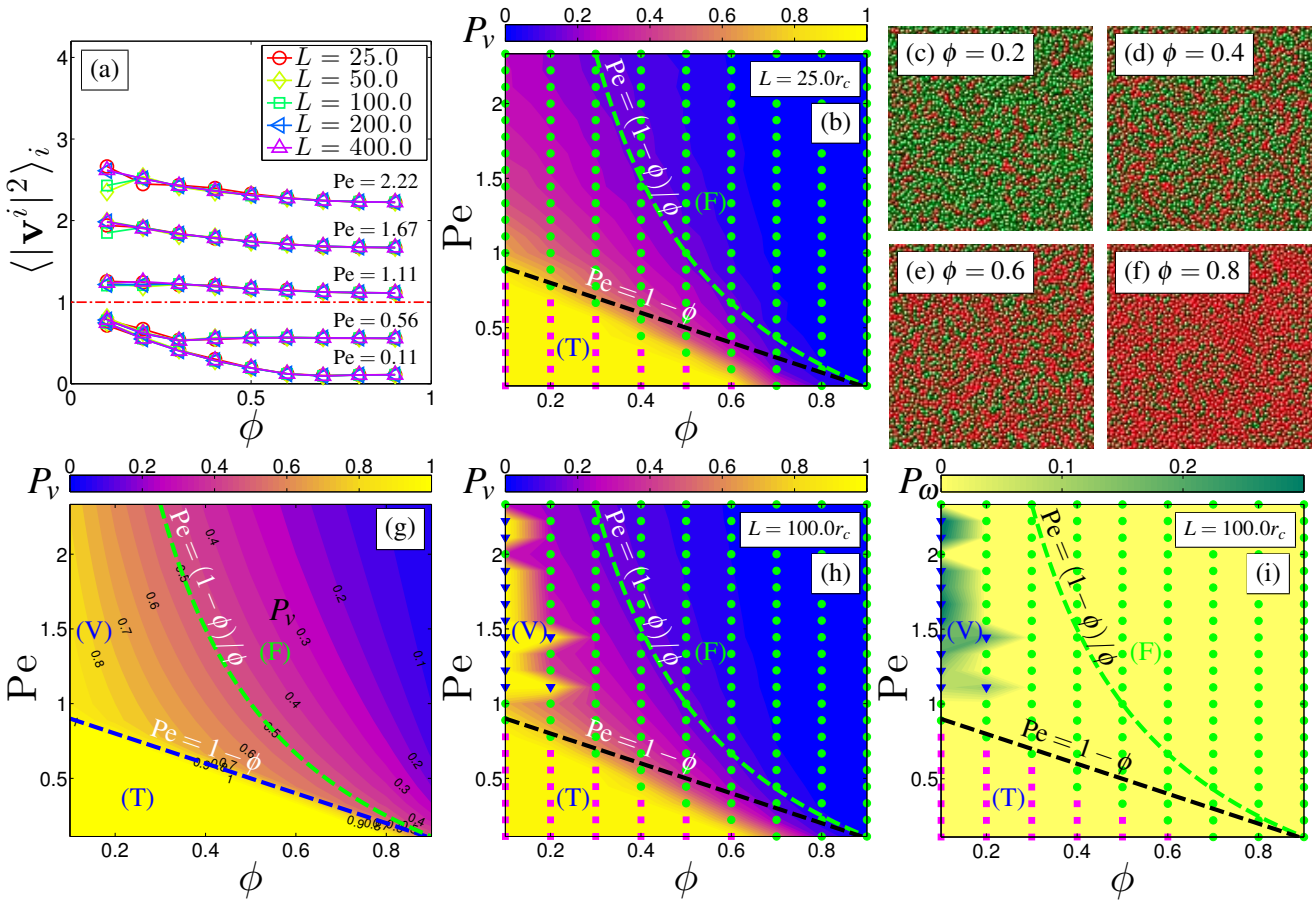

Fig. 2 Influence of the domain size, phase diagrams, and agent distribution fields. (a) Total kinetic energy $\langle |\mathbf{v}^i|^2 \rangle_i$ for different values of the linear domain size L. (b) P_v from simulations ($L = 25.0$). (c)–(f) Agent distribution fields. (g) P_v from theoretical estimates (14), (19), and (20). (h) P_v from simulations ($L = 100.0$). (i) P_ω from simulations ($L = 100.0$). The symbols ■, ▼, and ● distinguish, respectively, the mesoturbulent (T), the vortical (V), and the polar flocking (F) phases, as identified by the criteria appearing in Table 2.

For simplicity, we use a Gaussian filter with nondimensional filter width $\varepsilon = 15.0$. The order parameters P_v and P_ω are defined as

$$P_v = \frac{\langle |\mathbf{v}^i|^2 \rangle_i - \langle \mathbf{v}^i \rangle_i^2}{\langle |\mathbf{v}^i|^2 \rangle_i} \quad \text{and} \quad P_\omega = \langle |\omega|^2 \rangle - \langle \omega \rangle^2, \qquad (9)$$

where $\langle \cdot \rangle_i$ denotes the spatial average over all agents in the computational domain and $\langle \cdot \rangle$ denotes the spatial average over all points $\mathbf{x}_M$. Whereas P_v distinguishes between polar and non-polar states, P_ω distinguishes between non-polar phases exhibiting large-scale vortical motion and non-polar mesoturbulent phases. The associated limiting cases are summarized in Table 2. We determine the order parameters numerically and exhibit them as 2D contour plots in the (ϕ, Pe)–plane (Fig. 2). The phases in the (ϕ, Pe)–plane are marked using the identification criteria summarized in Table 2. To test for finite-size effects, we conducted all sets of simulations with different domain sizes ranging from $L = 25.0r_c$ to $L = 400.0r_c$. The vortical phase arises for small ϕ and $\mathrm{Pe} > 1$ in combination with large enough domain sizes (Fig. 2 (h) and (i)), whereas for the smallest domain size $r = 25.0r_c$ the vortical phase is absent (Fig. 2 (b)). The mesoturbulent phase appears to develop independently of the domain size in a triangular region enclosed by the origin, a point near $\phi \to 0$ and $\mathrm{Pe} \approx 1$, and a point near $\phi \to 1$ and $\mathrm{Pe} \to 0$. The total mean kinetic energy is found to coincide for all parameter combinations except those corresponding to the vortical phase (Fig. 2 (a)), which leads to the conclusion that the mesoturbulent and flocking phases are independent of the domain size. These results indicate that the vortical phase emerges only when the domain size is large enough to accommodate counterrotating vortices. Previous studies showed that an active suspension can be stabilized into a large-scale circulating state through appropriate confinement.[58,59] Further, the vortical phase in our simulations appears to resemble "milling" patterns observed in in-

vestigations of "pure" systems of self-motile agents with the flocking term (4).[49–54] Most remarkably, in our simulations the large-scale vortical patterns are found without the inclusion of stabilizing attractive forces or confining boundaries. Since the vortical phase occurs for small ϕ, the passive agents appear to play an important role in stabilizing vortical motion and point to the presence of effective hydrodynamic-like properties mediated through the presence of passive agents. This effect might be of key importance and deserves future investigation. However, in this article we focus on the transition criteria between the mesoturbulent phase and the flocking phase. Unless otherwise noted, the following discussion refers to simulations performed with $L = 100.0 r_c$.

Heuristically, the mesoturbulent phase is observed for parameter values of ϕ and Pe satisfying

$$\mathrm{Pe} \lesssim 1 - \eta\phi, \tag{10}$$

where η is an empirical parameter describing the slope of the line in the (ϕ, Pe)–plane below which the mesoturbulent phase prevails. To understand (10), consider the average kinetic energies, per agent, E_a and E_p corresponding to, respectively, active and passive agents. Heuristically, the mesoturbulent state emerges when the thermal kinetic energy of the passive agents exceeds the total energy (6) of the flocking state, namely when

$$E_p \gtrsim \frac{\alpha}{2\beta}. \tag{11}$$

In view of (2) and (5), the thermal equilibrium energy of the passive agents of the system is approximately

$$E_p \approx (1-\phi) k_B T. \tag{12}$$

As a consequence of (11) and (12), the mesoturbulent state emerges for

$$(1-\phi) k_B T \gtrsim \alpha/2\beta \tag{13}$$

or, equivalently, on invoking the definition (7) of Pe,

$$\mathrm{Pe} \lesssim 1 - \phi. \tag{14}$$

Comparison of (10) and (14) shows that the results from the numerical simulations agree qualitatively with the theoretical predictions and suggests that $\eta = 1$. However, the numerical results (Fig. 2 (b) and (h)) indicate that $\eta < 1$, resulting in transitions to the flocking phase for values of ϕ smaller than theoretically predicted. This effect can be explained by noting that the pairwise dissipative interactions between all agents result in an overall damping of the random fluctuations induced by the passive agents.

Next, we focus on the values of P_v around the transition between the mesoturbulent and the flocking phases. The contour lines in Fig. 2 (b) and (h) indicate a discontinuous transition between these phases, resulting in abrupt changes near a threshold value of $P_v \approx 0.5$. To determine the values of P_v for which transitions between the polar and non-polar states may be expected, consider the estimate of the energy in the polar state in terms of the mean velocity $\langle \mathbf{v}^i \rangle_i$ and the fluctuating velocity $\mathbf{v}^{i\prime} = \mathbf{v}^i - \langle \mathbf{v}^i \rangle_i$, such that, without loss of generality,

$$\tfrac{1}{2}\langle |\mathbf{v}^i|^2 \rangle_i = \tfrac{1}{2}\langle \mathbf{v}^i \rangle_i^2 + \tfrac{1}{2}\langle |\mathbf{v}^{i\prime}|^2 \rangle_i. \tag{15}$$

Whereas the flocking term drives polar order with a certain mean velocity, the passive agents are subject to random fluctuations. Hence, transitions between the mesoturbulent phase and the flocking phase may be expected when the fluctuations are large enough to break up the polar order with the mean velocity—i.e., when the energies associated with the mean velocity and fluctuations are equal:

$$\langle \mathbf{v}^i \rangle_i^2 = \langle |\mathbf{v}^{i\prime}|^2 \rangle_i. \tag{16}$$

By $(9)_1$, (15), and (16), we thus expect a transition between polar and non-polar phases near $P_v = 0.5$, which is consistent with the numerical results. In the flocking regime, P_v exhibits a nonlinear but continuous dependency on ϕ and Pe (Fig. 2 (b) and (h)). To understand how P_v depends on ϕ and Pe, we estimate values of P_v based on the relevant input parameters and compare them to numerical predictions. In the flocking regime, we estimate the terms entering the definition of the order parameter $(9)_1$ assuming that the contribution of energy due to the flocking forces of the active agents increases linearly with increasing ϕ and that the contribution of energy due to random fluctuations of the passive agents decreases linearly with increasing ϕ. Consequently, the total energy can be estimated as

$$\tfrac{1}{2}\langle |\mathbf{v}^i|^2 \rangle_i \approx \phi \frac{\alpha}{2\beta} + (1-\phi) k_B T, \tag{17}$$

while the energy associated with mean velocity can be estimated by

$$\tfrac{1}{2}\langle \mathbf{v}^i \rangle_i^2 \approx \phi \frac{\alpha}{2\beta}. \tag{18}$$

Notice that the estimate (17) is formally similar to a modified rule of mixtures between the characteristic flocking energy (6) and the characteristic energy (5) of random fluctuations. Consequently, bearing in mind the definition (7) of Pe, we find that

$$P_v \approx \frac{1-\phi}{\phi\,\mathrm{Pe} + 1 - \phi}. \tag{19}$$

Importantly, (19) provides an estimate for the order parameter P_v in the flocking regime of the (Pe, ϕ)–plane. In view of the previous discussion, the transition between the polar flocking phase and the disordered phase occurs at $P_v \approx 0.5$, yielding a criterion similar to (14):

$$\mathrm{Pe} \approx \frac{1-\phi}{\phi}. \tag{20}$$

The good qualitative agreement between the theoretically estimated phase diagram and the numerical predictions (Fig. 2 (g) and (h)) confirms the validity of the criteria (14), (19), and (20) derived from the energy estimates.

4 Mean-square displacement (MSD) and diffusion coefficients

The MSD $\langle(\Delta\mathbf{x}_i)^2\rangle_i = \langle(\mathbf{x}_i(\tau)-\mathbf{x}_{i_0})^2$ can be related to the diffusion through the Langevin equations. For a 2D system (cf., e.g., Metzler and Klafter[60])

$$\langle(\Delta\mathbf{x}_i)^2\rangle_i = 4D_\xi\tau^\xi, \tag{21}$$

where D_ξ is the coefficient associated with the power-law exponent ξ. For classical diffusive Brownian motion $\xi=1$ and D_1 is the diffusion coefficient,[61] whereas for ballistic motion $\xi=2$ and D_2 is proportional to a characteristic energy per unit mass. In the mesoturbulent phase, the present system exhibits ballistic motion at short times and diffusive motion at long times (Fig. 3 (a)). In experiments with 2D bacterial baths with tracer particles, Wu and Libchaber[7–9] observed a similar crossover from superdiffusive motion with $\xi>1$ to diffusive motion with $\xi\approx 1$. They found good fits of their experimental data with

$$\langle(\Delta\mathbf{x}_i)^2\rangle_i = 4D\tau(1-\exp(-\tau/\tau_c)), \tag{22}$$

where D is the diffusion coefficient and τ_c is the crossover time between two different asymtotic regimes; for $\tau\ll\tau_c$ the motion is ballistic and for $\tau\gg\tau_c$ the motion is diffusive. Least-squares fits of our simulation results (Fig. 3 (a)) show good agreement with (22), suggesting that the mesoturbulent phase exhibits statistical properties similar to those of 2D bacterial suspensions. Further, the diffusivity as well as the crossover time decrease with increasing ϕ, indicating that the random fluctuations of the passive agents are mainly responsible for the diffusivity of the mixtures and thus act as an effective solvent. At low ϕ, the diffusivity associated with the passive agents is significantly higher than the diffusivity associated with the active agents (Fig. 3 (a.I)). This difference in diffusivities decreases for increasing ϕ, signifying that the considered flocking mechanism effectively removes diffusivity, ultimately resulting in transitions to the polar flocking phase. Wu and Libchaber[7–9] determine effective long-time diffusion coefficients of

$$D_{e_{2.25\,\mu\mathrm{m}}} \approx 1.0\cdot 10^{-6}\,\mathrm{cm}^2/\mathrm{s} \tag{23}$$

and

$$D_{e_{5.0\,\mu\mathrm{m}}} \approx 4.3\cdot 10^{-7}\,\mathrm{cm}^2/\mathrm{s} \tag{24}$$

for bacteria baths with polystyrene (PS) tracer beads of radii $2.25\,\mu$m and $5.0\,\mu$m, respectively. To enable a direct comparison between the diffusion coefficients of the mesoturbulent phase (Fig. 3 (a.I)) and the experimental results of Wu and Libchaber,[7–9] we obtain the dimensionless counterparts of (23) and (24). Given a diffusion coefficient D_e carrying dimensions of length^2/time, we define a dimensionless diffusion coefficient D by

$$D = D_e\frac{1}{r_c}\left(\frac{m}{k_BT}\right)^{\frac{1}{2}}. \tag{25}$$

Now, for PS with density of $\rho_{\mathrm{PS}}\approx 10^3\,\mathrm{kg/m}^3$ and assuming that $T\approx 300\,\mathrm{K}$, we determine the dimensionless counterparts of (23) and (24) as

$$D_{2.25\,\mu\mathrm{m}}\approx 0.151 \quad\text{and}\quad D_{5.0\,\mu\mathrm{m}}\approx 0.097. \tag{26}$$

The dimensionless diffusion coefficients (26) are both within the range of diffusion coefficients of the mesuturbulent phase (Fig. 3 (a.I)) and correspond to the values occurring for low to intermediate values of ϕ in the mesoturbulent phase. This indicates that the diffusion properties of the mesoturbulent phase are not only qualitatively but also quantitatively similar to those of 2D bacterial suspensions.

In contrast to the mesoturbulent phase, the flocking phase exhibits ballistic behavior on all timescales (Fig. 3 (b)). Consistent with this, the MSD scales with τ^2. In the flocking phase, D_2 exhibits an increase with increasing ϕ, approaching what appears to be an asymptotic value for large ϕ (Fig. 3 (b.I)). To understand this limiting behavior, consider the MSD over time, which may be estimated to be proportional to the characteristic flocking energy per unit mass $\langle(\Delta\mathbf{x}_i)^2\rangle_i/\tau^2 \approx \alpha/\beta$. In view of (21), $D_2\approx\alpha/4\beta$ for ballistic motion in the flocking phase as shown by the dashed line in Fig. 3 (b.I). Further, the ballistic coefficients associated with the active and passive agents are almost identical. This confirms that, in the flocking regime, the flocking term dominates and drives the passive agents.

In the vortical phase, the system exhibits ballistic motion at short and intermediate times and diffusive motion at long times (Fig. 3 (c)). Notice that, in contrast to the data appearing in Fig. 3 (a)–(b), the results in Fig. 3 (c) appear for different representative Péclet numbers and $\phi=0.1$, since the vortical phase emerges only for low ϕ. Similarly as in the mesoturbulent phase, the fit to (22) provides good agreement with the data (Fig. 3 (c)). The crossover times to diffusive motion are an order of magnitude higher than those of the mesoturbulent phase (Fig. 3 (c.I)). This is consistent with the presence of a pair of counterrotating vortices and suggests that this structure is coherent for much longer times than the small-scale swirls that distinguish the mesoturbulent phase. The short-time ballistic coefficient exhibits a linear increase with increasing Pe (Fig. 3 (c.II)). Since the ballistic coefficient measures the characteristic energy per unit mass of the system, this demonstrates that the energy in the vortical phase depends linearly on Pe, even for small ϕ.

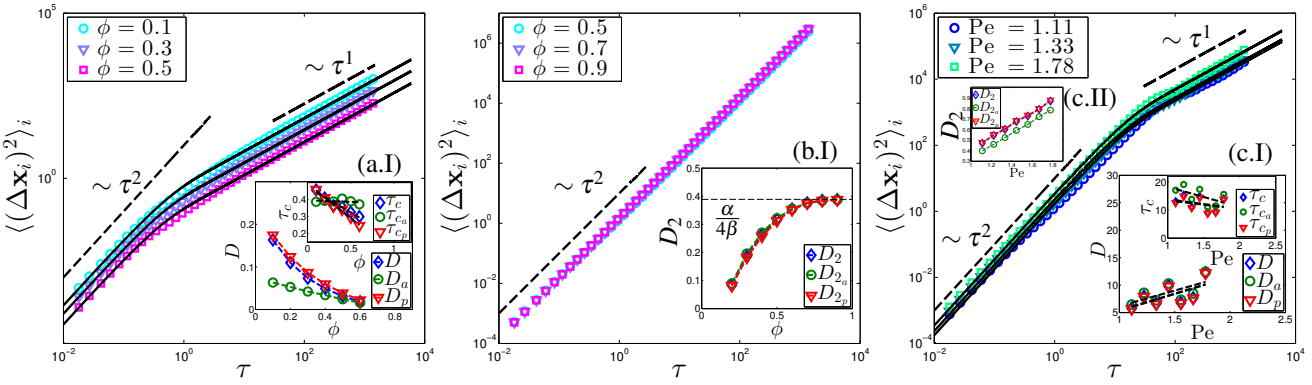

(a) Mesoturbulent phase (Pe = 0.11). **(b)** Flocking phase (Pe = 0.78). **(c)** Vortical phase ($\phi = 0.1$).

Fig. 3 MSD for the three different phases. D_a and t_{c_a} (D_p and t_{c_p}) denote the parameters associated with the active (passive) fraction of the mixture. (a) MSD for three different fractions of active agents (markers) along with least-squares fit to (22) indicated through solid lines. (a.I) Diffusion coefficients and crossover time obtained from a fit of the data to (22). (b) MSD for three different fractions of active agents. (b.I) Ballistic coefficients obtained from the relation (21) with $\xi = 2$. (c) MSD along with least-squares fit to (22) indicated through solid lines. (c.I) Short-time ballistic coefficients obtained from the relation (21) with $\xi = 2$ and (c.II) long-time diffusion coefficients as well as crossover time obtained from a fit of the data to (22).

5 Hydrodynamic effects?

In the continuum limit, the DPD method approximates Navier–Stokes-type hydrodynamics within certain limitations,[62] in particular on the Schmidt number $Sc = \mu/(\rho D)$, with μ the fluid viscosity and ρ the mass density.[48,63,64] Sc is a dimensionless measure of the competition between momentum diffusivity and mass diffusivity and is of order $O(1)$ for gases and of order $O(10^3)$ for liquids. Despite the Schmidt number of a DPD fluid being or order $O(1)$ rather than $O(10^3)$, DPD is expected to produce reasonable hydrodynamics in many applications,[65] granted suitable choices for the DPD parameters.

In the current study, we therefore use conventional DPD parameters. In the mesoturbulent phase, these parameter choices yield realistic diffusion properties, as discussed in Section 4. Yet, strategies to circumvent the Schmidt number limitations of DPD[66–68] might well result in improved results, in particular when the objective is to model a more detailed specific problem rather than a generic mixture as pursued in the current study. However, before tuning the Schmidt number limitations of DPD, more research needs to be done to determine whether "effective" Schmidt numbers can be defined for active matter and, secondarily, what impact modeling assumptions on the Schmidt number would have with regards to capturing the salient features of active matter.

Moreover, the impact of hydrodynamic effects in active matter is an ongoing research topic, as evidenced by recent publications[69,70] and reviews.[1] In particular, simulations suggest that purely steric interactions[1] can lead to large-scale correlated motion, whereas the effect of long-range hydrodynamic interactions remains controversial.[70] Importantly, in the current model, we do not prescribe any long-range interactions and we do not make any a priori assumptions on hydrodynamic interactions. Yet, our results suggest that in the mesoturbulent and the vortical phase, the passive agents act as an effective solvent mediating hydrodynamic like interactions, as discussed in Sections 3 and 4. In particular, the vortical phase appears to emerge due to effective hydrodynamic-like interactions between the active agents mediated by the presence of the passive agents, as discussed in Section 3. However, more detailed investigations of the hydrodynamic-like interactions in mixtures of active and passive agents would seem to be well worth the effort.

6 Discussion

The results of our model system have several implications that have potential to be further investigated within the context of both heterogeneous biological systems and heterogeneous artificial active matter systems. Artificial realizations of active matter systems include, for example, catalytically driven Janus particles,[35–39] light-activated particles,[40,41] polymer-based nanomotors,[42–44] and robotic swarms.[45–47] First, the results of our model system suggest that all dynamical phases and the associated motion patterns may be achieved using a relatively low fraction of self-motile agents. In scenarios where active matter is realized with artificial self-motile

agents, this implies that a small number of potentially difficult to manufacture and costly agents should suffice to drive passive agents and generate large-scale flow patterns. Further, it is conceivable that mixtures of active and passive particles have prospective value for microfluidic tasks such as pumping used in combination with confining geometries including, for example, ratchets.[71]

In a different scenario, the transition between mesoturbulent and the polar flocking phases might be controlled by adjusting the fraction of active agents, while fixing parameters associated with self-propulsion. Technologically, this means that the emergence of either phase could be controlled by switching identical agents on and off to adjust the fraction of active agents. Such a strategy would make it unnecessary to adjust the parameters related to the magnitude of the self-propulsion. The principle of controlling patterns of motion through using different species of active and passive particles might be used to increase efficiency in self-powered drug delivery systems,[72] water purification,[73] and a multitude of microfluidic processes. For example, the results of model system suggest that the concentration of (artificial) active agents could be used as a simple switch to control the onset of directed transport or pumping through a dynamical phase transition from the mesoturbulent phase to the flocking phase. This potentially promising avenue remains to be investigated experimentally. Moreover, the extent to which findings derived from our model system can be transferred to real systems of biological or artificial active matter remains to be decided.

7 Acknowledgements

We thank Pinaki Chakraborty, Gustavo Gioia, Russell Todres, and Steven Aird for helpful feedback and discussions on previous versions of the paper.

References

1 M. C. Marchetti, J. F. Joanny, S. Ramaswamy, T. B. Liverpool, J. Prost, M. Rao and R. A. Simha, *Rev. Mod. Phys.*, 2013, **85**, 1143.
2 D. van Ditmarsch, K. E. Boyle, H. Sakhtah, J. E. Oyler, C. D. Nadell, E. Déziel, L. E. P. Dietrich and J. B. Xavier, *Cell Rep.*, 2013, **4**, 697.
3 R. D. Monds and G. A. O'Toole, *Trends Microbiol.*, 2009, **17**, 73.
4 M. E. Hibbing, C. Fuqua, M. R. Parsek and S. B. Peterson, *Nature Rev. Microbiol.*, 2010, **8**, 15.
5 C. D. Nadell, K. R. Foster and J. B. Xavier, *PLoS Comput. Biol.*, 2010, **6**, e1000716.
6 J. B. Xavier, *Mol. Syst. Biol.*, 2011, **7**, 483.
7 X.-L. Wu and A. Libchaber, *Phys. Rev. Lett.*, 2000, **84**, 3017.
8 G. Grégoire, H. Chaté and Y. Tu, *Phys. Rev. Lett.*, 2001, **86**, 556.
9 X.-L. Wu and A. Libchaber, *Phys. Rev. Lett.*, 2001, **86**, 557.
10 G. Grégoire, H. Chaté and Y. Tu, *Phy. Rev. E*, 2001, **64**, 011902.
11 G. Miño, T. E. Mallouk, T. Darnige, M. Hoyos, J. Dauchet, J. Dunstan, R. Soto, Y. Wang, A. Rousselet and E. Clement, *Phys. Rev. Lett.*, 2011, **106**, 048102.
12 K. C. Leptos, J. S. Guasto, J. P. Gollub, A. I. Pesci and R. E. Goldstein, *Phys. Rev. Lett.*, 2009, **103**, 198103.
13 C. Valeriani, M. Li, J. Novosel, J. Arlt and D. Marenduzzo, *Soft Matter*, 2011, **7**, 5228.
14 L. Angelani, C. Maggi, M. L. Bernardini, A. Rizzo and R. Di Leonardo, *Phys. Rev. Lett.*, 2011, **107**, 138302.
15 S. R. McCandlish, A. Baskaran and M. F. Hagan, *Soft Matter*, 2012, **8**, 2527.
16 R. Ni, M. A. Cohen Stuart, M. Dijkstra and P. G. Bolhuis, *Soft Matter*, 2014, **10**, 6609.
17 N. Koumakis, A. Lepore, C. Maggi and R. Di Leonardo, *Nat. Commun.*, 2013, **4**, 2588.
18 N. Koumakis, C. Maggi and R. Di Leonardo, *Soft Matter*, 2014, **10**, 5695.
19 L. Angelani and R. Di Leonardo, *New J. Phys.*, 2010, **12**, 113017.
20 R. Di Leonardo, L. Angelani, D. Dell'arciprete, G. Ruocco, V. Iebba, S. Schippa, M. P. Conte, F. Mecarini, F. De Angelis and E. Di Fabrizio, *Proc. Natl. Acad. Sci. U. S. A.*, 2010, **107**, 9541.
21 A. Sokolov, M. M. Apodaca, B. A. Grzybowski and I. S. Aranson, *Proc. Natl. Acad. Sci. U. S. A.*, 2010, **107**, 969.
22 N. Darnton, L. Turner, K. Breuer and H. C. Berg, *Biophys. J.*, 2004, **86**, 1863.
23 E. Steager, C.-B. Kim, J. Patel, S. Bith, C. Naik, L. Reber and M. J. Kim, *Appl. Phys. Lett.*, 2007, **90**, 263901.
24 E. B. Steager, M. S. Sakar, D. H. Kim, V. Kumar, G. J. Pappas and M. J. Kim, *J. Micromech. Microeng.*, 2011, **21**, 035001.
25 B. Behkam and M. Sitti, *Appl. Phys. Lett.*, 2007, **90**, 023902.
26 D. Kim, A. Liu, E. Diller and M. Sitti, *Biomed. Microdevices*, 2012, **14**, 1009.
27 R. Fernandes, M. Zuniga, F. R. Sassine, M. Karakoy and D. H. Gracias, *Small*, 2011, **7**, 588.
28 D. B. Weibel, P. Garstecki, D. Ryan, W. R. DiLuzio, M. Mayer, J. E. Seto and G. M. Whitesides, *Proc. Natl. Acad. Sci. U. S. A.*, 2005, **102**, 11963.
29 X. Fu, L.-H. Tang, C. Liu, J.-D. Huang, T. Hwa and P. Lenz, *Phys. Rev. Lett.*, 2012, **108**, 198102.
30 C. Liu, X. Fu, L. Liu, X. Ren, C. K. L. Chau, S. Li, L. Xiang, H. Zeng, G. Chen, L.-H. Tang, P. Lenz, X. Cui, W. Huang, T. Hwa and J.-D. Huang, *Science*, 2011, **334**, 238.
31 J. Stricker, S. Cookson, M. R. Bennett, W. H. Mather, L. S. Tsimring and J. Hasty, *Nature*, 2008, **456**, 516.
32 R. McDaniel and R. Weiss, *Curr. Opin. Biotechnol.*, 2005, **16**, 476.
33 L. You, R. Sidney Cox III, R. Weiss and F. H. Arnold, *Nature*, 2004, **428**, 868.
34 H. Kobayashi, M. Kaern, M. Araki, K. Chung, T. S. Gardner, C. R. Cantor and J. J. Collins, *Proc. Natl. Acad. Sci. U. S. A.*, 2004, **101**, 8414.
35 W. F. Paxton, A. Sen and T. E. Mallouk, *Chem. Eur. J.*, 2005, **11**, 6462.
36 N. Mano and A. Heller, *J. Am. Chem. Soc.*, 2005, **127**, 11574.
37 J. G. Gibbs and Y.-P. Zhao, *Appl. Phys. Lett.*, 2009, **94**, 163104.
38 H.-R. Jiang, N. Yoshinaga and M. Sano, *Phys. Rev. Lett.*, 2010, **105**, 268302.
39 G. Volpe, I. Buttinoni, D. Vogt, H.-J. Kümmerer and C. Bechinger, *Soft Matter*, 2011, **7**, 8810.
40 J. Palacci, S. Sacanna, A. P. Steinberg, D. J. Pine, and P. M. Chaikin, *Science*, 2013, **339**, 936.
41 J. A. Cohen and R. Golestanian, *Phys. Rev. Lett.*, 2014, **112**, 068302.
42 Y.-G. Tao and R. Kapral, *ChemPhysChem*, 2009, **10**, 770.
43 R. Kapral, *J. Chem. Phys.*, 2013, **138**, 020901.
44 Z. Wu, Y. Wu, W. He, X. Lin, J. Sun and Q. He, *Angew. Chem.*, 2013, **52**, 7000.
45 L. Giomi, N. Hawley-Weld and L. Mahadevan, *Proc. R. Soc. A*, 2013, **469**, 20120637.
46 H. Li and H. P. Zhang, *Europhys. Lett.*, 2013, **102**, 50007.
47 M. Rubenstein, A. Cornejo, and R. Nagpal, *Science*, 2014, **345**, 795.

48 R. D. Groot and P. B. Warren, *J. Chem. Phys.*, 1997, **107**, 4423.

49 H. Levine, W.-J. Rappel and I. Cohen, *Phys. Rev. E*, 2000, **63**, 017101.

50 M. R. D'Orsogna, Y. L. Chuang, A. L. Bertozzi and L. S. Chayes, *Phys. Rev. Lett.*, 2006, **96**, 104302.

51 Y.-L. Chuang, M. R. D'Orsogna, D. Marthaler, A. L. Bertozzi and L. S. Chayes, *Phys. D*, 2007, **232**, 33.

52 Y.-L. Chuang, Y. R. Huang, M. R. D'Orsogna and A. L. Bertozzi, IEEE International Conference on Robotics and Automation, Roma, Italy, 10-14 April 2007, 2007.

53 J. Carrillo, M. D'Orsogna and V. Panferov, *Kinet. Relat. Models*, 2009, **2**, 363.

54 J. A. Carrillo, M. Fornasier, G. Toscani and F. Vecil, *Mathematical Modeling of Collective Behavior in Socio-Economic and Life Sciences, Modeling and Simulation in Science, Engineering and Technology*, Birkhäuser, Boston, 2010, pp. 297–336.

55 S. Plimpton, *J. Comput. Phys.*, 1995, **117**, 1.

56 LAMMPS (Large-scale Atomic/Molecular Massively Parallel Simulator), *http://lammps.sandia.gov*, 2013.

57 L. Verlet, *Phys. Rev.*, 1967, **159**, 98.

58 F. G. Woodhouse and R. E. Goldstein, *Phys. Rev. Lett.*, 2012, **109**, 168105.

59 H. Wioland, F. G. Woodhouse, J. Dunkel, J. O. Kessler and R. E. Goldstein, *Phys. Rev. Lett.*, 2013, **110**, 268102.

60 R. Metzler and J. Klafter, *Phys. Rep.*, 2000, **339**, 1.

61 A. Einstein, *Ann. Phys.*, 1905, **17**, 549.

62 P. Español, *Phys. Rev. E*, 1995, **52**, 1734.

63 V. Symeonidis, G. E. Karniadakis and B. Caswell, *J. Chem. Phys.*, 2006, **125**, 184902.

64 Z. Li and G. Drazer, *Phys. Fluids*, 2008, **20**, 103601.

65 E. Moeendarbary, T. Y. Ng and M. Zangeneh, *Int. J. Appl. Mechanics*, 2009, **1**, 737.

66 J. M. Kim and R. J. Phillips, *Chem. Eng. Sci.*, 2004, **59**, 4155.

67 S. Chen, N. Phan-Thien, B. C. Khoo and X. J. Fan, *Phys. Fluids*, 2006, **18**, 103605.

68 D. A. Fedosov, I. V. Pivkin and G. E. Karniadakis, *J. Comput. Phys.*, 2008, **227**, 2540.

69 A. Lefauve and D. Saintillan, *Phys. Rev. E*, 2014, **89**, 021002.

70 E. Lushi, H. Wioland and R. E. Goldstein, *Proc. Natl. Acad. Sci. U. S. A.*, 2014, **111**, 9733.

71 P. K. Ghosh, V. R. Misko, F. Marchesoni and F. Nori, *Phys. Rev. Lett.*, 2013, **110**, 268301.

72 D. Patra, S. Sengupta, W. Duan, H. Zhang, R. Pavlick and A. Sen, *Nanoscale*, 2013, **5**, 1273.

73 L. Soler, V. Magdanz, V. M. Fomin, S. Sanchez and O. G. Schmidt, *ACS Nano*, 2013, **7**, 9611.

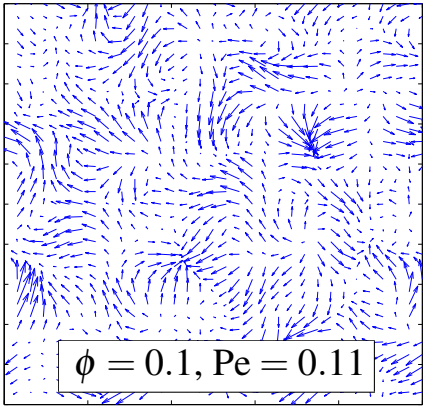
Mesoturbulent
$\phi = 0.1$, Pe $= 0.11$

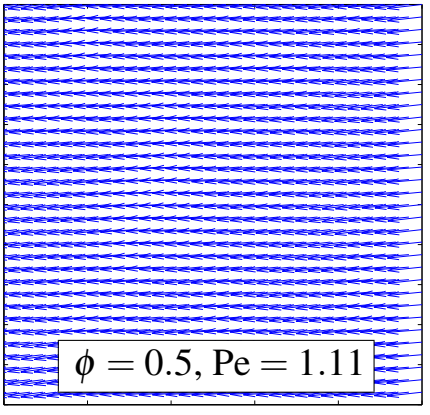
Polar flock
$\phi = 0.5$, Pe $= 1.11$

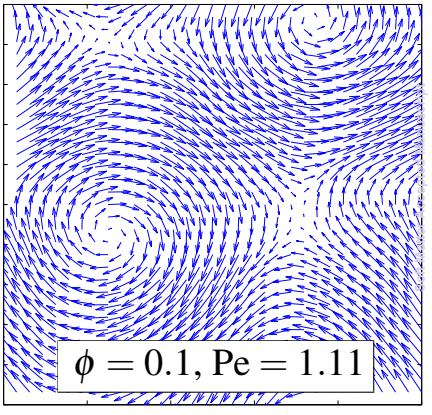
Vortical
$\phi = 0.1$, Pe $= 1.11$

We model mixtures of self-motile and passive agents and study dynamical phases and diffusion properties.